Supporting Information

Dual-Anchored Configuration Involving on $Pb(NO_3)_2$ for Effective and Stable $FAPbI_3$ Quantum Dot Solar Cells

Meidan Que,[a] Shenghui He,[a] Lili Gao,[*b] Boyue Zhang,[a] Yabo Wang,[a] Jin Chen,[a] Bo Li,[a] Wei Huang,[c] Peng Zhong[*d]

[a] *College of Materials Science and Engineering, Xi'an University of Architecture and Technology, Xi'an 710055, P. R. China.*

[b] *College of Metallurgical Engineering, Xi'an University of Architecture and Technology, Xi'an 710055, P. R. China.*

[c] *College of Civil Engineering, Xi'an University of Architecture and Technology, Xi'an 710055, P. R. China.*

[d] *School of Advanced Materials and Nanotechnology, Xidian University, Xi'an, 710126, P. R. China.*

*** Corresponding Author:**

Lili Gao, E-mail: gll0706@xauxt.edu.cn

Peng Zhong, E-mail: pengzhong@xidian.edu.cn

Table of Contents

Supplementary Figures

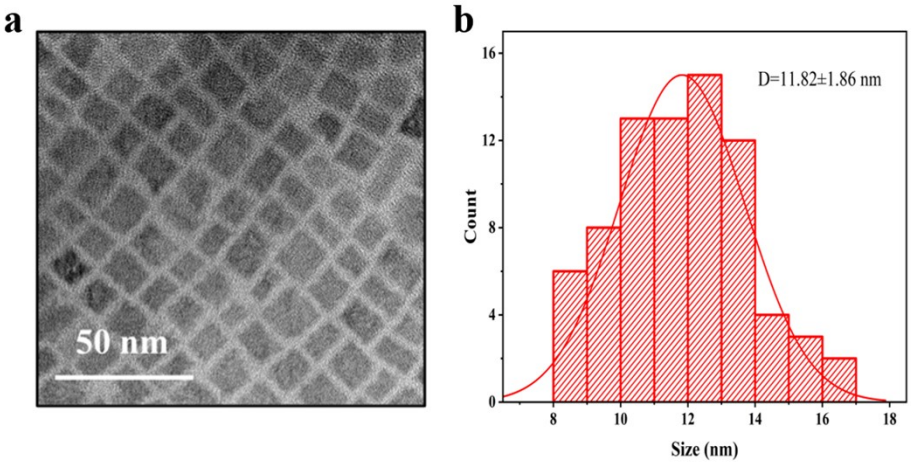

Fig. S1 (a) TEM image and (b) the corresponding size distribution of $FAPbI_3$ quantum dots.

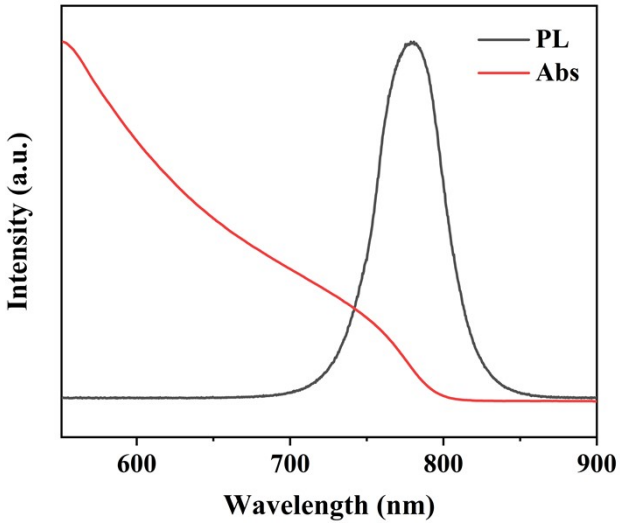

Fig. S2 The UV- visible absorption and steady-state PL spectrum of $FAPbI_3$ quantum dot solution in hexane.

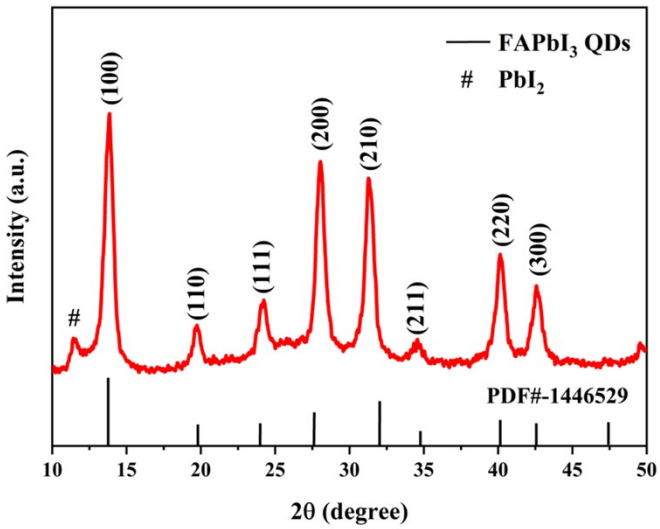

Fig. S3 XRD pattern of $FAPbI_3$ quantum dot solution.

The XRD was further applied to explore the possible variations of the crystal structure of $FAPbI_3$ quantum dot. As shown in **Fig. S3**, the three main diffraction peaks at 13.8°, 28.0° and 42.6° correspond to the typical diffraction peaks of the (100), (200) and (210) lattice planes of $FAPbI_3$ quantum dots, respectively. This demonstrates the integrity of the crystal structure of the prepared quantum dots.

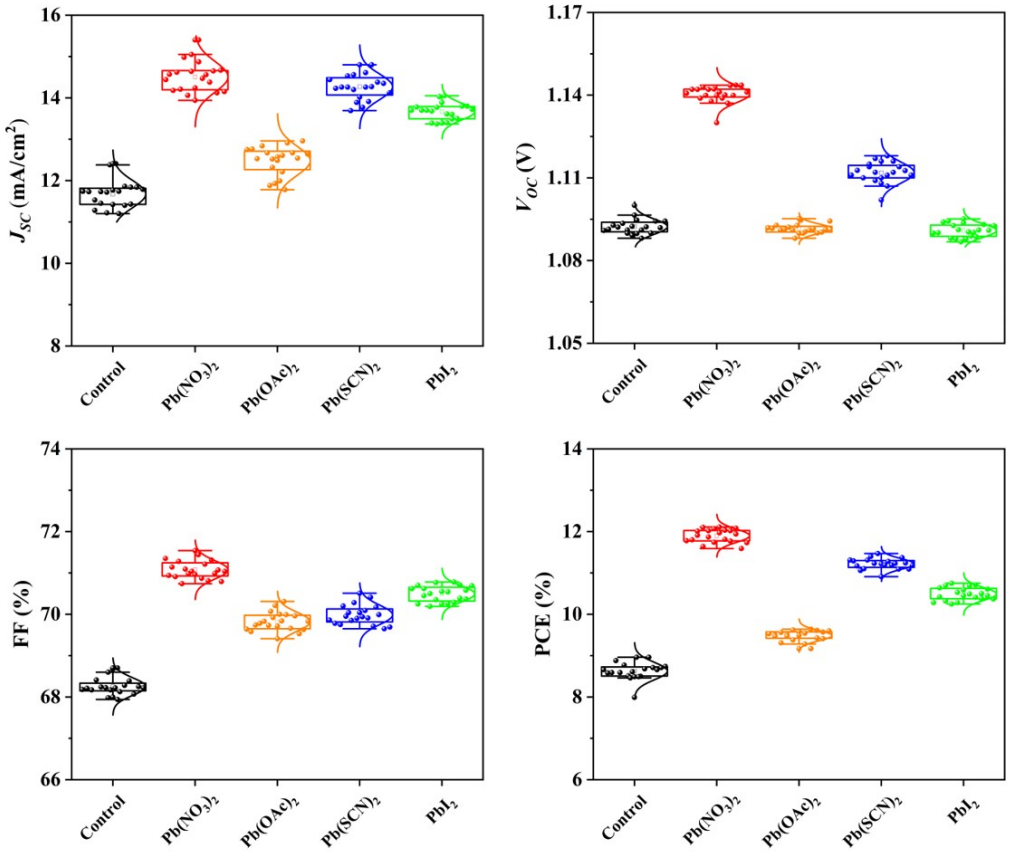

Fig. S4 Photovoltaic performance evolutions (J_{SC}, V_{OC}, FF, and PCE) of $FAPbI_3$ quantum dot solar cells using four kinds of Pb-salts (Control, $Pb(NO_3)_2$, $Pb(OAc)_2$, PbI_2, $Pb(SCN)_2$).

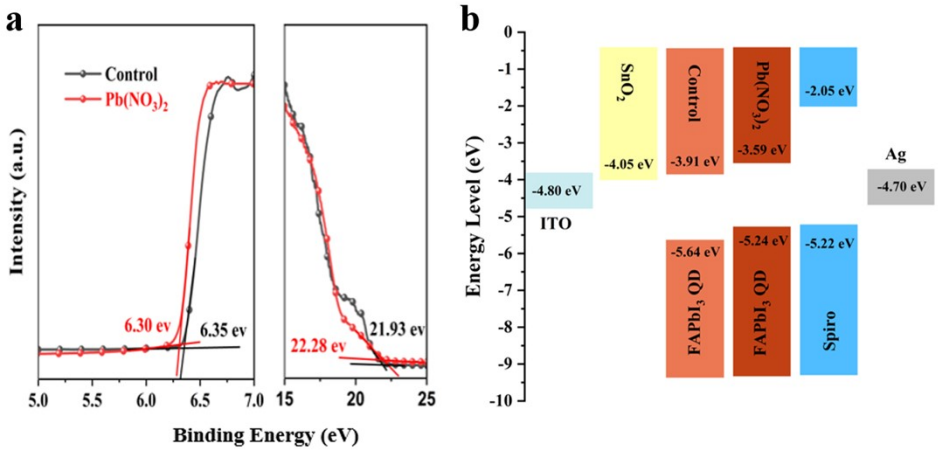

Fig. S5 (a) UPS spectra of w/wo $Pb(NO_3)_2$ posttreatment quantum dot films and (b) the correponding energy band positions for $FAPbI_3$ quantum dot solar cell.

UPS measurement is used to calculate the energy levels of original and $Pb(NO_3)_2$-based solid films. The position of the valence band top is calculated by the following formula:[S1]

$$E_{Homo} = -(h_v - E_{cutoff} + E_{VBF}) \quad \text{(Eq. 1)}$$

Where h_v、E_{cutoff} and E_{VBF} in the formula represent photon energy, secondary electron cutoff energy, and injection barrier in turn. The calculated E_{Homo} values are -5.64 eV, and -5.24 eV for control and $Pb(NO_3)_2$-based film, respectively. The energy level values of SnO_2 and 2,2',7,7'-tetrakis(N,N-di-p-methoxyphenylamine)-9,9'spirobifluorene(SpiroOMeTAD) were obtained from the literature.[错误!未找到引用源。] We can see that the positions of VBM and CBM of $Pb(NO_3)_2$-based film are slightly upward than the original control film in **Fig. S5b**, which leads to a more favorable energy level arrangement inside the perovskite solar cell. This favorable energy level arrangement can promote the extraction of charge carriers.[S1]

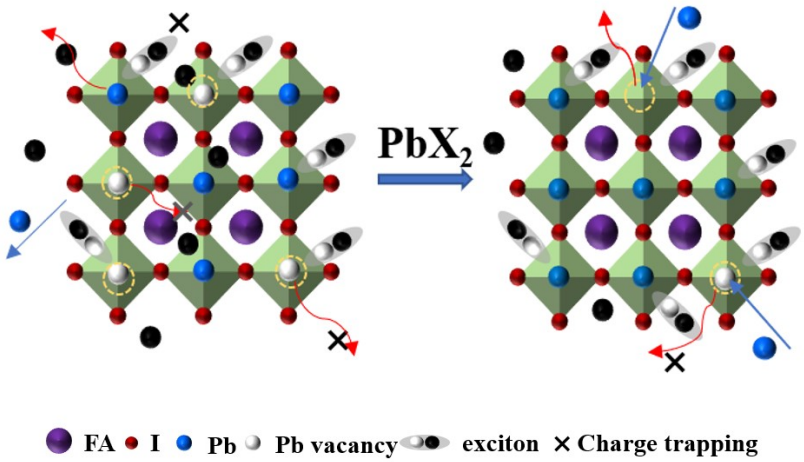

Fig. S6 Mechanism passivation for $FAPbI_3$ quantum dot.

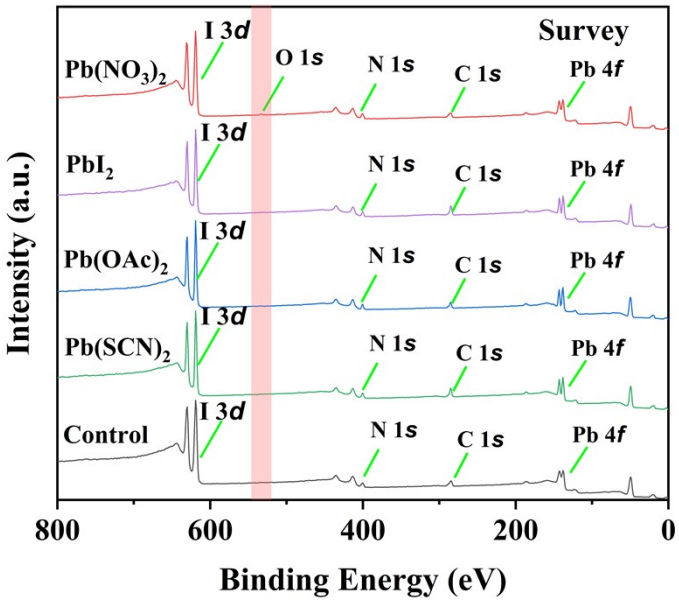

Fig. S7 Survey XPS spectra of $FAPbI_3$ quantum dot films w/wo lead salt post-treatment.

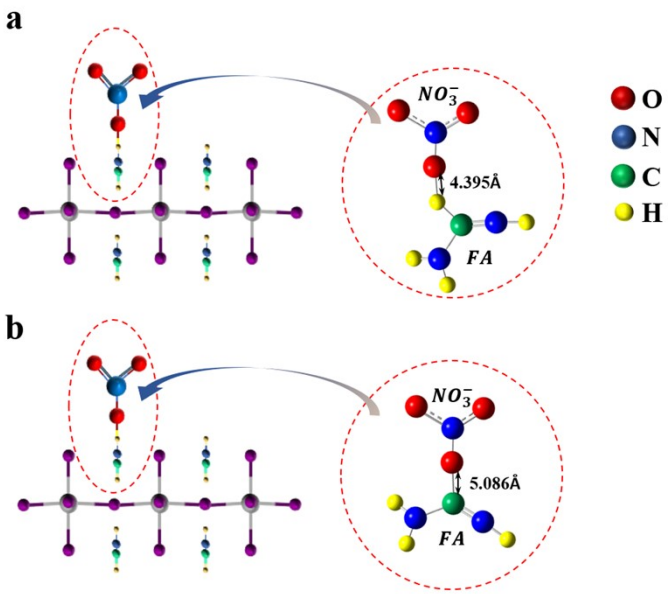

Fig. S8 The optimized geometries of single-anchored crystal structure calculated by DFT calculation: (a) O-H and (b) O-C.

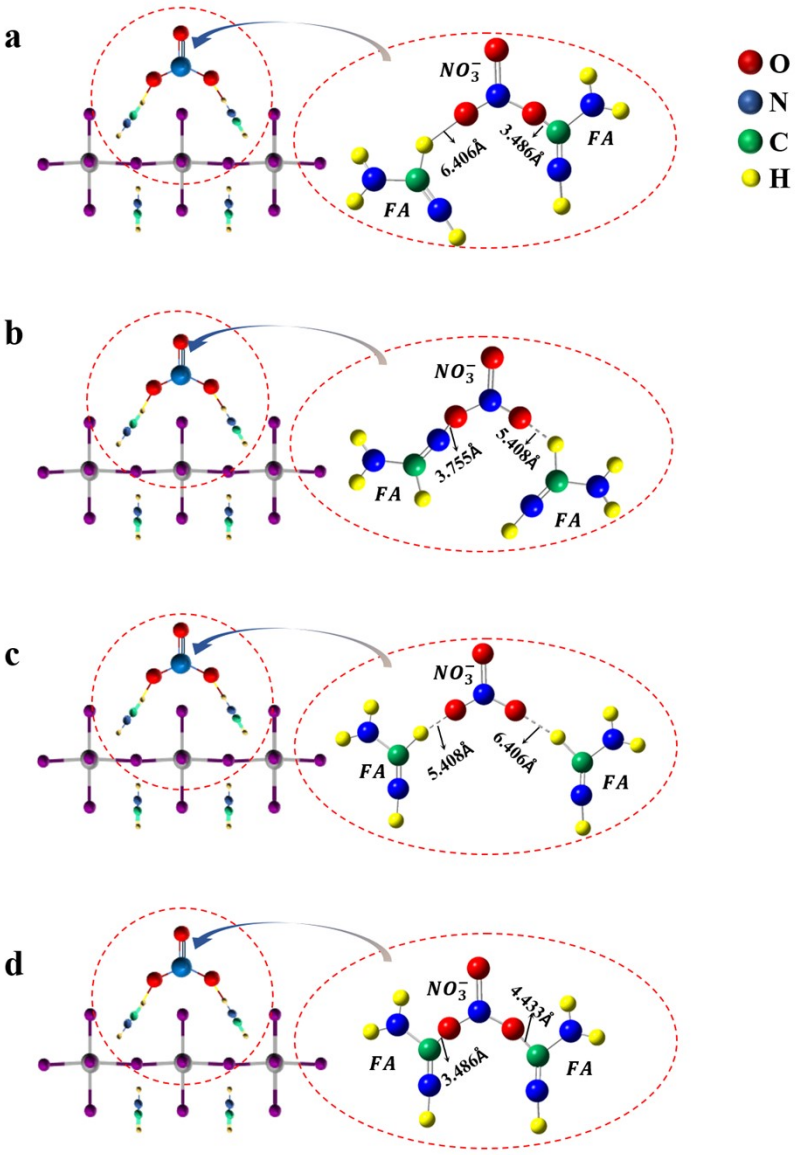

Fig. S9 The optimized geometries of double-anchored crystal structures by DFT calculation: (a) O-H···O-C, (b) O-H···O-N, (c) O-H···O-H, (d) O-C···O-C.

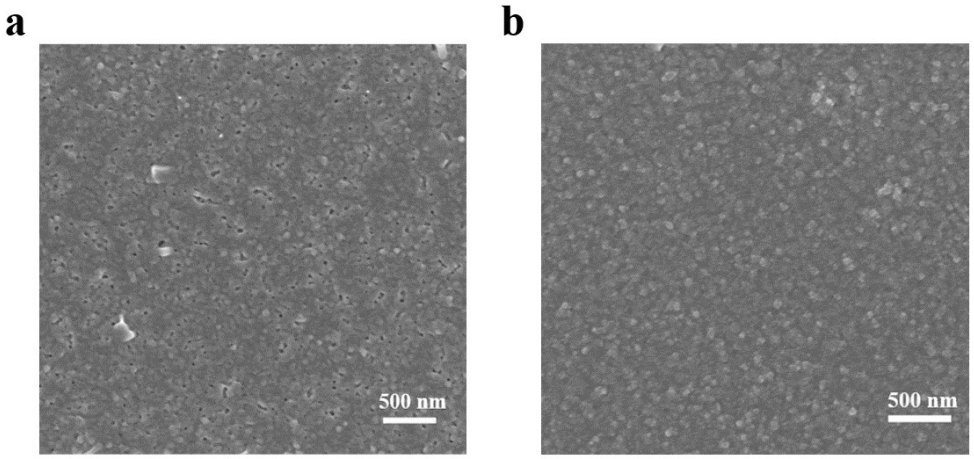

Fig. S10 (a) and (b) SEM images of $FAPbI_3$ quantum dot films w/wo $Pb(NO_3)_2$ posttreatment.

To investigate the effect of $Pb(NO_3)_2$ additives on grain growth, the surface morphology of $FAPbI_3$ quantum dot films were meticulously examined employing scanning electron microscopy (SEM). In **Fig. S10**, reveal that the $Pb(NO_3)_2$-based film exhibits a denser array of quantum dots with significantly fewer pinholes compared to the control film. This notable enhancement can be attributed to a multitude of contributory factors. Principally, the introduction of $Pb(NO_3)_2$ alters the surface chemistry of perovskite quantum dots by supplying essential Pb ions, building a Pb-rich environment. This facilitates tighter packing of crystals, consequently reducing both the porosity and defect density within the film. Additionally, $Pb(NO_3)_2$ undergoes chemical reactions with the FA^+ ions present within the $FAPbI_3$ quantum dots, forming new chemical bonds that enhance the adhesion and density of the film. Additionally, owing to the inherently dynamic nature of halide perovskite quantum dots, the post-treatment regimen with nitrate salts triggers a partial recrystallization phenomenon on the surfaces thereof.

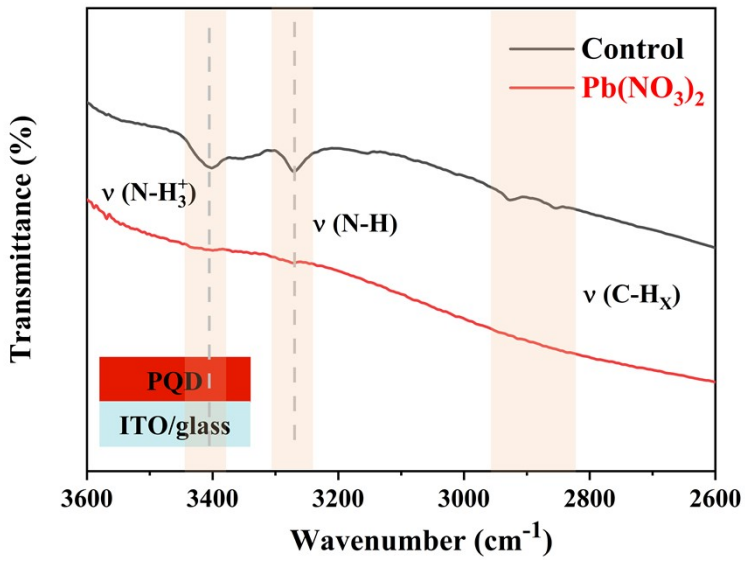

Fig. S11 FTIR spectra of $FAPbI_3$ quantum dot films w/wo $Pb(NO_3)_2$ post-treatment.

The surface chemistry environment of quantum dot films w/wo $Pb(NO_3)_2$ post-treatment was first characterized by Fourier transform infrared (FTIR). As displayed in **Fig. S11**, the peaks at 3403 cm^{-1} and 3272 cm^{-1} can be attributed to $N\text{-}H_3^+$ and N-H scissor bending in oleylamine, and the peak at 2930 cm^{-1} and 2858 cm^{-1} are ascribed to the $C\text{-}H_X$ scissor bending in oleic acid, are observed for the control films.[S2] For $Pb(NO_3)_2$-based film, the peaks described above almost disappear, which indicates that $Pb(NO_3)_2$ facilitates the removal of oleic acid and oleylamine ligands, thereby fabricating an excellent surface chemical environment for the quantum dot film.

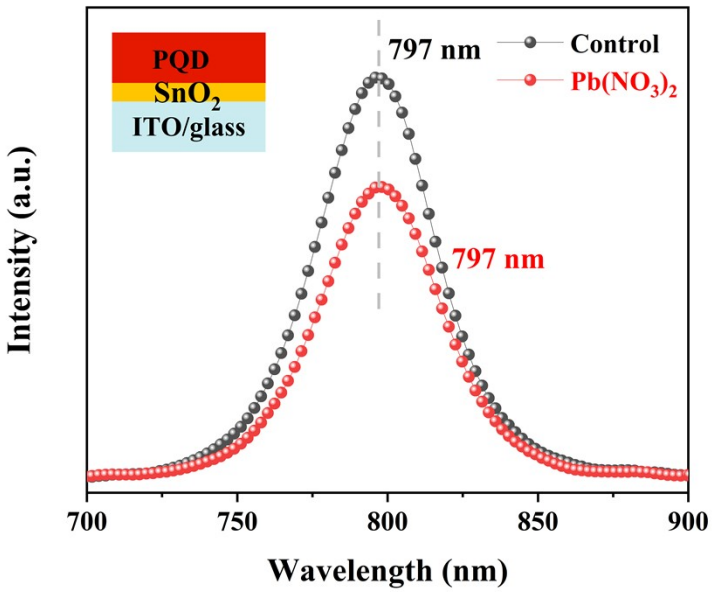

Fig. S12 PL spectra with electron transport layer of $FAPbI_3$ quantum dot films w/wo $Pb(NO_3)_2$ post-treatment.

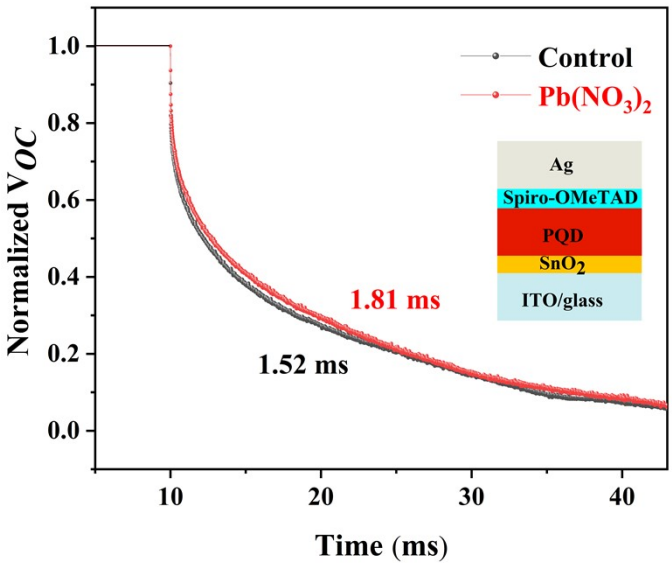

Fig. S13 TPV curve of $FAPbI_3$ quantum dot devices w/wo $Pb(NO_3)_2$ post-treatment.

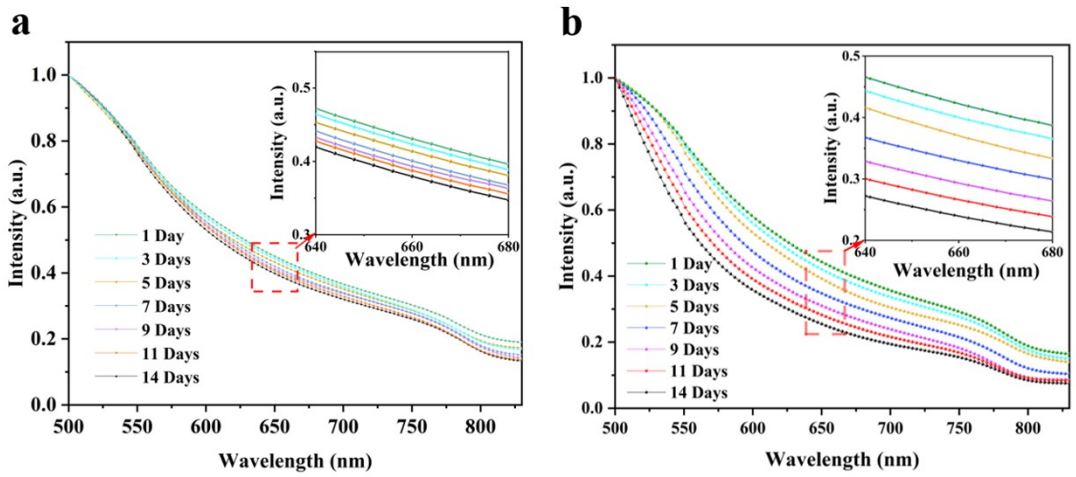

Fig. S14 (a) and (b) Absorption spectra stabilities of $FAPbI_3$ quantum dot films w/wo $Pb(NO_3)_2$ posttreatment.

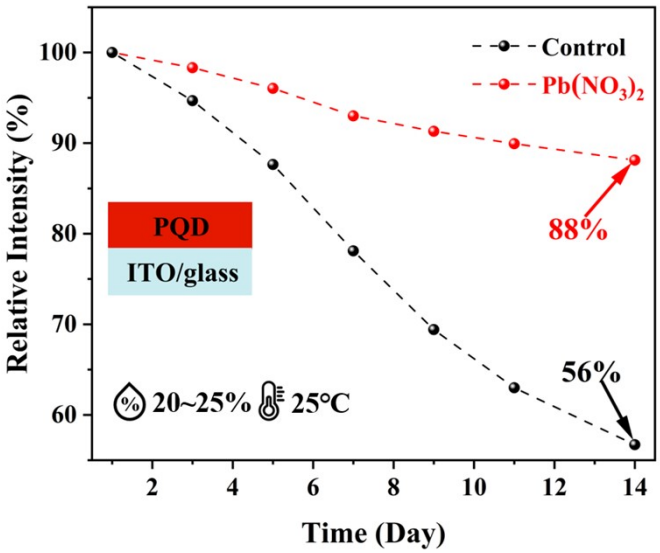

Fig. S15 The corresponding relative absorption stabilities upon humidity of 20 % and room temperature at 660 nm.

To verify the stability of $FAPbI_3$ quantum dot films with double-anchored structure, the stability of control and $Pb(NO_3)_2$-based films under ambient conditions of 25 % humidity was evaluated (**Fig. S14**). The absorbance of the $Pb(NO_3)_2$-based film maintains its initial 78% at 660 nm after 14 days, while the control film decreases to 54%, as shown in **Fig. S15**. The absorbance attenuation of the control film is significantly faster than that of the $Pb(NO_3)_2$-based film. These results reveal that the stability of quantum dot films is significantly improved after repairing the surface defects of V_{Pb2+} and V_{FA+}.

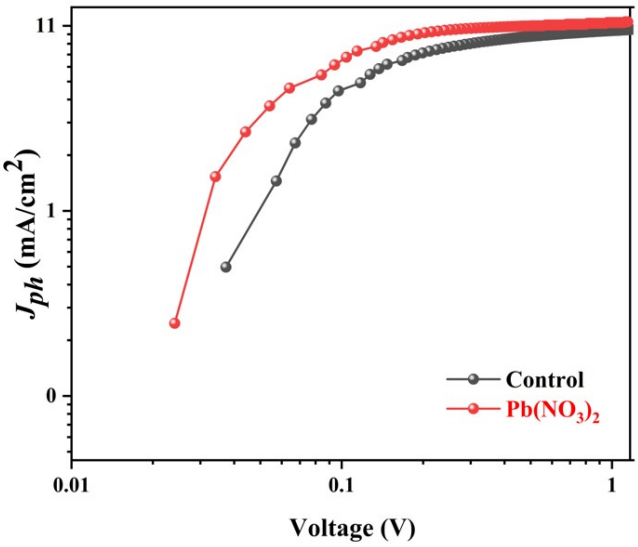

Fig. S16. J_{ph}-V_{eff} curves of the $FAPbI_3$ quantum dot solar cell w/wo $Pb(NO_3)_2$ posttreatment.

The relationship between photocurrent density (J_{ph}) and effective voltage (V_{eff}) is a common indicator for assessing the charge carrier extraction efficiency in photovoltaic devices. The J_{ph} is defined as $J_{ph} = J_{light} - J_{dark}$, and V_{eff} is expressed as $V_{eff} = V_0 - V_a$, wherein V_0 represents the voltage when $J_{ph} = 0$ mA cm^{-2}, and V_a is applied as the bias voltage. With a growth in V_{eff}, J_{ph} linearly increases in the low V_{eff} region and then becomes saturated in the high V_{eff} region. Saturated J_{ph} represents the photogenerated carrier collected by the electrode at the low bias voltage stage.[S3] **Fig. S16** shows that the J_{ph} of the $Pb(NO_3)_2$-based device is higher than the control device, indicating more efficient carrier extraction and transport in the former, which also contributes to the higher current density.

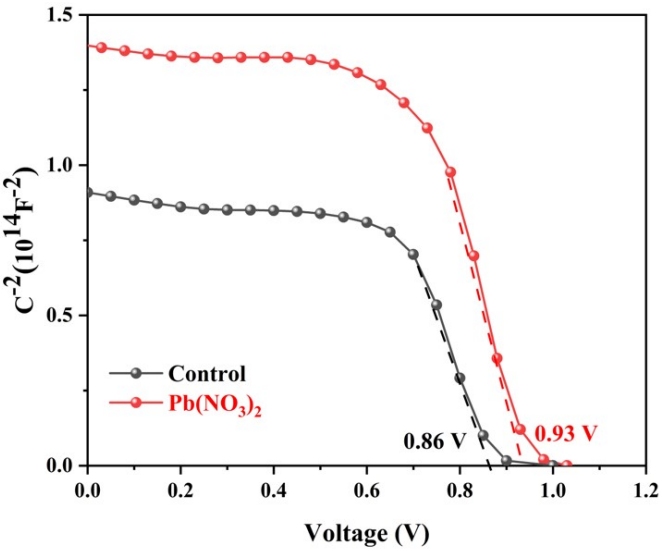

Fig. S17. Mott-Schottky fitting to the C-V data of the $FAPbI_3$ quantum dot solar cells w/wo $Pb(NO_3)_2$ post-treatment.

The reduced trap density in solid quantum dot films could also impact the built-in potential (V_{bi}) of PQDSCs, which is crucial for the extraction of charge carriers in PQDSCs. As shown in **Fig. S17**, the V_{bi} of the $Pb(NO_3)_2$-based device is much higher than that of the control device. The enhanced V_{bi} is more beneficial in promoting charge separation and preventing carrier recombination, thus improving the charge collection efficiency of cells.

Theoretical calculations

Table S1 The calculated binding energies and interatomic distances in the optimized structures.

Bonding mode	Binding Energy (eV)	Distance (Å)
C-O	-7.46	5.086
N-O	-8.93	3.861
H-O	-8.89	4.395
H-O	-9.25	6.406
O-H		5.408
C-O	-10.04	3.486
O-C		4.430
C-O	-9.49	3.486
O-H		6.406
N-O	-9.1	3.755
O-H		5.408
N-O	-10.51	3.775
C-O		3.486

Table S2 TRPL paraments of w/wo $Pb(NO_3)_2$ of $FAPbI_3$ quantum dot films.

Sample	A_1	τ_1 (ns)	A_2	τ_2 (ns)	τ_{ave} (ns)
Control	65.77	10.28	12.18	70.79	44.20
$Pb(NO_3)_2$	46.12	14.11	13.80	74.92	51.44

The PL decay was fitted using the following equation,[S4]

$$\mathbf{I(t) = A_1 \cdot exp\left(-\frac{t}{\tau_1}\right) + A_2 \cdot exp\left(-\frac{t}{\tau_2}\right) + A_0} \quad \text{(Eq. 2)}$$

where $\mathbf{A_0}$, $\mathbf{A_1}$ and $\mathbf{A_2}$ are constants, $\mathbf{t}$ is PL decay time, $\boldsymbol{\tau}$ is the fitted lifetime. The average lifetime (τ_{ave}) was calculated by the following equation,[S4]

$$\boldsymbol{\tau_{ave} = \frac{A_1\tau_1^2 + A_2\tau_2^2}{A_1\tau_1 + A_2\tau_2}} \quad \text{(Eq. 3)}$$

Table S3 TPC paraments of w/wo $Pb(NO_3)_2$ of $FAPbI_3$ quantum dot films.

Sample	A_1	τ_1 (μs)
Control	1.31×10^6	2.98
$Pb(NO_3)_2$	2.39×10^8	2.17

The fitted function for J_{SC} decay is shown in Eq. 4,[S5]

$$J_{SC} = A_1 \cdot \exp\left(-\frac{t}{\tau_1}\right) + A_0 \quad \text{(Eq. 4)}$$

where A_0 and A_1 are constants, t is J_{SC} decay time, τ_1 is the fitted lifetime.

Table S4 TPV paraments of w/wo $Pb(NO_3)_2$ of $FAPbI_3$ quantum dot films.

Sample	A_1	τ_1 (ms)	A_1	τ_2 (ms)	τ_{ave} (ms)
Control	142.25	1.24	0.19	17.00	1.52
$Pb(NO_3)_2$	86.65	1.35	0.20	17.47	1.81

The fitted function of TPV curves is shown in Eq. 5,[S6]

$$V_{OC} = A_1 \cdot \exp\left(-\frac{t}{\tau_1}\right) + A_2 \cdot \exp\left(-\frac{t}{\tau_2}\right) + A_0 \quad \text{(Eq. 5)}$$

where A_0, A_1 and A_2 are constants, t is V_{OC} decay time, τ is the fitted lifetime. The average lifetime (τ_{ave}) was calculated by the following equation,

$$\tau_{ave} = \frac{A_1\tau_1^2 + A_2\tau_2^2}{A_1\tau_1 + A_2\tau_2} \quad \text{(Eq. 6)}$$

Supporting References

S1 C. Zhang, X. Yin, G. Chen, Z. Sang, Y. Yang, W. Que, *ACS Photonics*, 2023, **10**, 790-800.

S2 J. Yuan, C. Bi, J. Xi, R. Guo, J. Tian, *J. Phys. Chem. Lett.*, 2021, **12**, 1018-1024.

S3 W. Zhu, Q. Zhang, D. Chen, Z. Zhang, Z. Lin, J. Chang, J. Zhang, C. Zhang, Y. Hao, *Adv. Energy Mater.*, 2018, **8**, 1802080.

S4 X. Fu, T. He, S. Zhang, X. Lei, Y. Jiang, D. Wang, P. Sun, D. Zhao, H.-Y. Hsu, X. Li, M. Wang, M. Yuan, *Chem*, 2021, **7**, 3131-3143.

S5 X. Zhang, J. Zhang, D. Phuyal, J. Du, L. Tian, V. A. Öberg, M. B. Johansson, U. B. Cappel, O. Karis, J. Liu, *Adv. Energy Mater.*, 2018, **8**, 1702049.

S6 L. Zhang, C. Kang, G. Zhang, Z. Pan, Z. Huang, S. Xu, H. Rao, H. Liu, S. Wu, X. Wu, *Adv. Funct. Mater.*, 2021, **31**, 2005930.